Journal of Pharmacy

JOP
Journal of Pharmacy

# Green Synthesis of Silver Nanoparticles Using *Aidia densiflora* Leaf Extract: Characterisation and Bioactivities

Ainul Hayati Zeheri[1], Muhammad Taher[1*], Muhammad Taufiq Mohd Jailani[1], Juliana Md Jaffri[1], Deny Susanti[2], Junaidi Khotib[3]

[1]*Department of Pharmaceutical Technology, Kulliyyah of Pharmacy, International Islamic University Malaysia, Jalan Sultan Ahmad Shah, 25200 Kuantan, Pahang, Malaysia.*
[2]*Department of Chemistry, Kulliyyah of Science, International Islamic University Malaysia, Jalan Sultan Ahmad Shah, 25200 Kuantan, Pahang, Malaysia.*
[3]*Department of Pharmacy Practice, Faculty of Pharmacy, Airlangga University, 60115 Surabaya, Indonesia.*

## Abstract

**Introduction:** Plant-mediated green synthesis of nanoparticles has become a promising option in green nanotechnology because it is simple, cost-effective, eco-friendly, and biologically effective. This study focused on the synthesis and characterisation of silver nanoparticles (AgNPs) using *Aidia densiflora* leaf extract, as well as the evaluation of their antimicrobial and cytotoxic activities. **Methods:** AgNPs were synthesised with *A. densiflora* leaf extract and their formation was confirmed using an ultraviolet–visible (UV–Vis) spectrophotometer. Liquid chromatography-mass spectrometry quadrupole time-of-flight was utilised for phytochemical profiling. The synthesised AgNPs were characterised using a zetasizer and zeta potential analyser, scanning electron microscopy-energy dispersive X-ray, Fourier Transform Infrared, X-ray diffraction (XRD), and thermogravimetric analysis. Antimicrobial activity of AD-AgNPs was tested against six microorganisms using the disc diffusion method, while cytotoxicity against MCF-7 human breast cancer cells was evaluated via MTT assay. **Results:** AgNP formation was confirmed by XRD and UV–Vis analysis, with absorbance peaks at 399–424 nm. Optimal synthesis was achieved using 10 mM $AgNO_3$ at 60°C and pH 7. SEM showed spherical-like nanoparticles averaging 96.06 nm with significant aggregation. The zeta potential was –35.6 mV, and XRD indicated a face-centred cubic structure with a crystalline size of 6.94 nm. AD-AgNPs showed no antimicrobial activity and low cytotoxicity. **Conclusion:** *A. densiflora* leaf extract can be used to synthesise AgNPs, however, further optimisation is required for better nanoparticle stabilisation and improvement of bioactivities.

**Article history:**

Received: 28 February 2025
Accepted: 2 July 2025
Published: 31 July 2025

**Keywords:**

Metal nanoparticles
*Aidia densiflora*
Plant-mediated synthesis
Antimicrobial
Cytotoxicity

doi: 10.31436/jop.v5i2.390

*Corresponding author's email: mtaher@iium.edu.my

## Introduction

Nanotechnology has gained significant attention as a new research area due to its diverse applications in biomedicine, pharmaceuticals, electrochemistry, catalysis, food technology, sensors, cosmetics, and more. Nanoparticles are atomic- or molecular-scale solid particles with a size of <100 nm (Vanlalveni et al., 2021). The conversion of bulk materials to nanoparticles has demonstrated the enhancement of the properties of the parent materials due to high atomic interactions, owing to their large surface area-to-volume ratio (Singh et al., 2018). several metallic nanoparticles, such as silver nanoparticles (AgNPs), have gained significant momentum for their potential as antimicrobial agents. AgNPs have proven to be very useful, especially in the biomedical field for their antimicrobial, antibiofilm, antifungal, antiparasitic, antioxidative, and anticancer activity. Their applications have been found in topical ointments, wound dressings, ultrasound gels, bone cements, surgical implants, and medical devices because of their antimicrobial nature (Velidandi et al., 2020).

Nanoparticles have been more commonly synthesised using physical and chemical methods, which require expensive equipment, use toxic chemicals, and release hazardous by-products. The production of nanoparticles through physical and chemical methods can be toxic to both humans and the environment, which also limits their applications (Akhter et al., 2024). Therefore, researchers have developed new approaches to green synthesis of nanoparticles by utilisation of biologically friendly elements such as bacteria, viruses, yeasts, plant extracts, fungi, and algae (Singh et al., 2018). In comparison to the various green synthesis methods for metal and metal oxide nanoparticles, plant extract-based synthesis is a simpler, more efficient, and scalable approach compared to microbial methods (Singh et al., 2018). Biomolecules in plant extracts, such as polyphenols, amino acids, vitamins, enzymes, and proteins, play an important role as both reducing and stabilising agents in the stages of nanoparticle synthesis (Asif et al., 2022). Numerous studies have been conducted on the synthesis of AgNPs using various plant extracts; however, no research has yet been conducted on *Aidia densiflora* in this area.

To date, no studies have explored the phytochemical constituents, antioxidant properties, or bioactive compounds of *A. densiflora*. However, research on related species within the same genus had demonstrated the presence of various phytochemical compounds, such as alkaloids, triterpenoids, flavonoids, and coumarins, which can potentially act as reducing and stabilising agents in AgNP synthesis (Anokwah et al., 2021; Awang-Jamil et al., 2019). Additionally, *A. densiflora* grows abundantly across Malaysia, making it readily available and cost-effective for this research. This study aimed to synthesise AgNPs using *A. densiflora* leaf extract, characterise the nanoparticles, and evaluate their antimicrobial and cytotoxic activities. The antimicrobial efficacies were assessed against two Gram-positive bacteria (*Bacillus subtilis*, *Staphylococcus aureus*), two Gram-negative bacteria (*Pseudomonas aeruginosa*, *Escherichia coli*), and two fungi (*Candida albicans* and *Aspergillus niger*) using the disc diffusion method, while the cytotoxicity study was conducted on MCF-7 (human breast cancer cells) using the MTT assay.

## Materials and Methods

### *Materials*

Fresh leaves of *Aidia densiflora* (Wall.) Masam (Fig. 1) were collected from Kuantan, Pahang, Malaysia in October 2024 and identified by Dr. Shamsul Khamis. The plant specimen was then deposited in the Herbarium of the Kulliyyah of Pharmacy, IIUM Kuantan, Malaysia. The test microorganisms included *Bacillus subtilis, Staphylococcus aureus, Pseudomonas aeruginosa, Escherichia coli, Candida albicans,* and *Aspergillus niger* obtained from ATCC, US. MCF-7, human breast cancer cells also obtained from ATCC, US. Silver nitrate ($AgNO_3$, EMSURE®, Merck, analytical grade), dimethyl sulfoxide (DMSO, EMSURE®, Merck, analytical grade), ethanol (EMSURE®, Merck, analytical grade), methanol (EMSURE®, Merck, analytical grade), sodium hydroxide (NaOH, R&M Chemicals), 3-(4,5-Dimethylthiazol-2-

yl)-2,5-diphenyltetrazolium bromide (MTT reagent, Molecular Probes), tamoxifen citrate (Calbiochem, Merck), econazole nitrate (Dr. Ehrenstorfer), kanamycin sulphate (Sigma-Aldrich), amoxicillin/clavulanic acid disc (Oxoid, Thermo Fisher) were used as chemical reagents.

Dulbecco's Modified Eagle's Medium (DMEM, Gibco), TrypLE Express (Gibco), Fetal Bovine Serum (FBS, Gibco), Penicillin-Streptomycin (Nacalai Tesque, Kyoto, Japan), phosphate-buffered saline (PBS, Sigma-Aldrich), Tryptic Soy Agar and Tryptic Soy Broth (TSA, TSB, Merck), Nutrient Agar and Nutrient Broth (NA, NB, Merck), Sabouraud Dextrose Agar and Sabouraud Dextrose Broth (SBA, SDB, Merck) were used for microbial and cytotoxic studies. The instruments used included a ultraviolet–visible spectrophotometer (Shimadzu UV-1800), LC-MS/QTOF (Agilent 1200 LC system coupled with a 6520 QTOF mass spectrometer, Agilent Technologies), FTIR spectrometer (PerkinElmer Dual), scanning electron microscope with energy dispersive X-ray (SEM, JEOL / JSM-IT200), zetasizer nano (Malvern ZN1600 Nano ZS), X-ray diffractometer (XRD, ULVAC-PHI / PHI 5000 VersaProbe II), thermogravimetric analysis (TGA, Hitachi / STA7000), high-speed centrifuge (Supra 22K, Hanil Science Industrial), microplate reader (Azure Biosystems), rotary evaporator (BÜCHI Rotavapor R-300) and sonicator (Qsonica). Other apparatus included were Petri dish (90 mm × 15 mm), $CO_2$ incubator (BB15, Thermo Fisher, 5% $CO_2$, 37°C) and 96-well flat-bottom tissue culture plates (Falcon, Becton Dickinson).

***Method***

*Collection of plant material and extraction*

Fresh *A. densiflora* leaves were dried at 40°C and ground into powder. 50 g of the dried powder was mixed with 500 mL of 80% ethanol (Eze et al., 2019) and extracted using ultrasonic-assisted extraction (UAE) with a probe sonicator at 50 kHz for 30 minutes. The extract was filtered through filter paper, followed by 0.45 µm and 0.22 µm syringe filters, and stored at 4°C.

**Fig. 1**: *A. densiflora* plant collected from Kuantan, Pahang, Malaysia.

*Liquid chromatography-mass spectrometry time of flight (LC-MS/QTOF) analysis*

The *A. densiflora* leaf extract was dried using a rotary evaporator at 50°C, diluted to 1 mg/mL in methanol, and filtered through a 0.22 µm syringe filter before injection. Chromatographic separation was conducted on an Agilent ZORBAX Eclipse Plus C18 column (2.1 × 100 mm, 1.8 µm) at 40°C. The mobile phase consisted of 0.1% formic acid in deionized water (A) and 0.1% formic acid in acetonitrile (B), with a gradient elution over 30 minutes at a 0.25 mL/min flow rate. The mass spectrometer operated in positive ESI mode with a gas temperature of 325°C, gas flow of 11 L/min, and nebulizer pressure of 35 psi. Data analysis was performed using Agilent Mass Hunter Qualitative Analysis B.05.00 software based on accurate mass measurements.

*Synthesis of Aidia densiflora-silver nanoparticle (AD-AgNP)*

AgNPs were synthesised at a 1:9 ratio (extract solution: $AgNO_3$), as a previous optimisation study by Jalab et al. (2021) demonstrated effective AgNPs formation at this ratio. 10 mL of plant extract was added dropwise to 90 mL of 1-, 5-, and 10-mM silver nitrate ($AgNO_3$) solution under constant stirring at 60°C for 2 hours. The formation of AgNPs was monitored through periodic sampling using a UV spectrophotometer. As reported by Alharbi et al. (2022), numerous studies have shown that AgNPs production increases with higher pH levels, with the highest yield achieved at a pH range of 7–9. Therefore, the sample with the highest absorbance peak among the three $AgNO_3$ concentration

variable was used to further investigate the effect of different pH levels on AgNPs formation. The same method was applied, keeping other variables constant. After the 2 hours synthesis, the mixture was adjusted to pH levels of 7, 8, and 9 by adding 1 M NaOH dropwise and stirred for another 30 minutes at room temperature. The final mixture was centrifuged at 8000 rpm for 10 minutes at 21°C. The pellet was rinsed by removing the supernatant, adding distilled water, and centrifuging again. This rinsing step was repeated three times.

*Characterisation of AD-AgNPs*

*Ultraviolet–visible (UV-Vis) spectrophotometric analysis*

During the reaction, 1 mL of the sample solution was analysed using a UV-Vis spectrophotometer (Shimadzu UV-1800) to confirm AgNPs formation. Wavelength and absorbance were recorded within a 300–800 nm scanning range, with distilled water as the blank. Samples were appropriately diluted to ensure absorbance readings fell within the optimal range.

*Particle size and zeta potential analysis*

The size, polydispersity index (PDI), and zeta potential value of the synthesised AgNPs was determined using a zetasizer instrument (Malvern ZN1600 Nano ZS).

*Scanning electron microscopy-energy dispersive X-ray (SEM-EDX) analysis*

The semi-solid AD-AgNPs were deposited on a glass slide, dried, and gold-coated using a vacuum sputter coater. The morphology, size, and elemental composition of the synthesised AD-AgNPs were examined using an SEM-EDX analyser (JEOL /JSM-IT200) at 20 kV. This method was retrieved from Sundar et al. (2024).

*X-ray diffractometer (XRD) analysis*

XRD analysis was conducted to assess the crystallinity, phase, and average crystallite size of AD-AgNPs using XRD (ULVAC-PHI / PHI 5000 VersaProbe II). The analysis was performed using CuK$\alpha$ radiation ($\lambda$ = 1.5405 Å) over a 2$\theta$ range of 20°–100°, with an accelerating voltage of 45 kV and an applied current of 40 mA. The average crystallite size (D) was calculated using the Debye-Scherrer equation: $D = K\lambda/\beta \cos \theta$, where K is the Scherrer constant (0.9), $\lambda$ is the X-ray wavelength (1.5405 Å), $\beta$ is the full width at half maximum (FWHM) in radians, and $\theta$ is the diffraction angle.

*Thermogravimetric analysis (TGA)*

The dried powder of the AD-AgNPs was subjected to TGA using TGA (Hitachi / STA7000) under a nitrogen atmosphere with a flow rate of 10 mL/min. The sample was heated from room temperature to 700 °C at a heating rate of 10 °C/min.

*Fourier Transform Infrared (FTIR) analysis*

FTIR analysis was conducted to identify functional groups and biomolecules involved in AgNPs synthesis. Spectra were recorded using FTIR spectrometer (PerkinElmer Dual) in the range of 4000–400 $cm^{-1}$ in Attenuated Total Reflectance (ATR) mode.

*Antimicrobial assay*

The antimicrobial activity of AD-AgNPs was assessed using the disc diffusion assay against two Gram-positive bacteria (*B. subtilis*, *S. aureus*), two Gram-negative bacteria (*E. coli*, *P. aeruginosa*), and two fungi (*C. albicans*, *A. niger*). Bacteria were inoculated on nutrient agar and incubated at 37 °C for 24 hours, while *C. albicans* and *A. niger* were cultured on TSA and Sabouraud dextrose agar at 35 °C for 5 days. The bacteria were then subcultured in nutrient broth, *C. albicans* in TSB, and *A. niger* in Sabouraud dextrose broth under the same conditions. The turbidity of all cultures was standardised to ~$1.5 \times 10^8$ CFU/mL by adjusting UV absorbance at 625 nm to 0.08–0.1 (Arsène et al., 2023; Karu et al., 2020; Safarpoor et al., 2018)

Test samples included 10 mg/mL and 5 mg/mL AD-AgNPs, 5 mg/mL *A. densiflora* leaf extract, 5 mg/mL $AgNO_3$, and distilled water as a negative control. All samples were sterilised using a 0.22 μm syringe filter. Sterile discs were immersed in the samples and placed on the plates (Safarpoor et al., 2018). Amoxicillin-clavulanate and econazole discs were used as positive controls for antibacterial and antifungal assays, respectively (Pallavi et al., 2022; Safarpoor et al., 2018). Plates were incubated at 37 °C for 24 hours (bacteria) and at 35 °C for 5 days (fungi), after which the zone of inhibition (ZOI) was

measured in mm. The assay was conducted in duplicate.

*Cytotoxic activity*

The MTT assay was performed to evaluate the cytotoxic activity of AD-AgNPs and $AgNO_3$ against MCF-7 cells. The cells were first cultured in tissue culture flasks with complete medium consisting of Dulbecco's Modified Eagle Medium (DMEM) supplemented with 10% (v/v) foetal bovine serum (FBS) and 1% (v/v) penicillin-streptomycin, then incubated at 37°C in a 5% $CO_2$ atmosphere. Once the cells reached 80% confluence, trypsinisation was performed to detach them from the flasks. Subsequently, the cells were seeded into a 96-well plate at a density of $2 \times 10^4$ cells/well and incubated for 24 hours. Following incubation, the cells were treated with serially diluted AD-AgNPs, $AgNO_3$, and tamoxifen (positive control) at concentrations of 5, 2.5, 1.25, 0.625, and 0.312 mg/mL, then further incubated at 37°C in 5% $CO_2$ for 24 hours. Afterwards, 10 µL of MTT solution (5 mg/mL) and 90 µL of complete medium were added to each well, and the plate was re-incubated for 4 hours. In this step, viable cells with active mitochondria converted MTT into purple formazan crystals. To dissolve the crystals, 100 µL of dimethyl sulfoxide (DMSO) was added, followed by an additional 30-minute incubation in the $CO_2$ incubator.

Absorbance was measured at 570 nm using a microplate reader. Higher absorbance indicated greater cell viability (lower cytotoxicity), whereas lower absorbance suggested reduced viability (higher cytotoxicity). The percentage of cell viability was calculated using the following formula:

$$\text{Cell viability (\%)} = \frac{(\text{OD of treated cells})}{(\text{OD of control cells})} \times 100 \qquad (1)$$

OD = optical density

This method was adapted from Fadhillah et al. (2024).

*Statistical analysis*

Statistical analysis was conducted using Jamovi. Data from the tests were reported as mean ± standard deviation (SD). One-way ANOVA was performed to determine significant differences, with $p < 0.05$ considered statistically significant.

## Results and Discussion

*LC-MS/QTOF based profiling of A. densiflora extract*

**Fig. 2** presents the LC-MS profile of *A. densiflora* leaf extract, identifying 99 compounds, with 12 considered major (≥1% volume).

**Fig. 2** presents the LC-MS profile of *A. densiflora* leaf extract, identifying 99 compounds, with 12 considered major (≥1% volume). Among them, only 4 compounds are known, while the remaining 8 remain unidentified as presented in **Table 1**. According to Nguyen et al. (2023), active phytochemicals such as phenolics, terpenoids, flavones, alkaloids, amino acids, polysaccharides, and alcoholic compounds may contribute to the reduction of AgNPs by donating electrons to convert $Ag^+$ to $Ag^0$. Similarly, Zuhrotun et al. (2023) highlighted the role of polyphenols as the reducing and stabilising agents in AgNPs formation. Among the major compounds detected, the polyphenolic compounds epifisetinidol-4α-ol, 1,3,4,5-tetracaffeoylquinic acid, and proanthocyanidin A5′ are likely key contributors to AgNP formation. Additionally, minor constituents in the extract (≤1% volume) may further support the synthesis process, either by enhancing the reduction efficiency or improving nanoparticle stability.

*Characterisation of AD-AgNPs*

Visual observation

The addition of *A. densiflora* extract to the $AgNO_3$ solution resulted in colour changes, indicating the formation of AgNPs. As shown in **Fig. 3**, the extract initially exhibited a deep green colour (a), which turned light yellow (b) upon mixing with $AgNO_3$. Over time, the solution gradually changed to brown (c), becoming darker as the reaction progressed. This change suggests the reduction of $Ag^+$ ions and the excitation of surface plasmon resonance (SPR). Further adjustment of the pH using sodium hydroxide resulted in a deep brown colour (g), indicating potential effects on nanoparticle stability and growth. These observations align with previous studies by Liaqat et al. (2022) and Asif et al. (2022), that correlate colour changes with AgNPs synthesis.

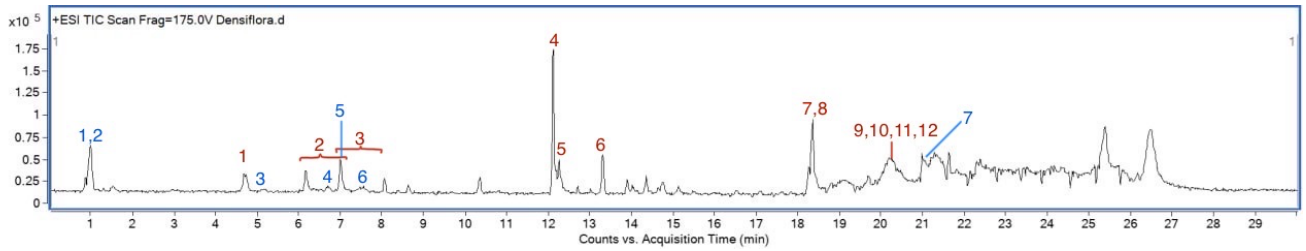


**Fig. 2.** LC-MS profile of *A. densiflora* leaf extract. Chromatographic separation was conducted on an Agilent ZORBAX Eclipse Plus C18 column (2.1 × 100 mm, 1.8 µm) at 40°C. The mobile phase consisted of 0.1% formic acid in deionized water (A) and 0.1% formic acid in acetonitrile (B), with a gradient elution over 30 minutes at a 0.25 mL/min flow rate. The mass spectrometer operated in positive ESI mode with a gas temperature of 325°C, gas flow of 11 L/min, and nebulizer pressure of 35 psi. Compounds are labeled based on their relative abundance: Red labels: major compounds with a percentage

**Table 1:** Compounds identified in LC-MS analysis.

| No. | RT | Name of Compound | Formula | Mass | Volume (%) | Classification |
|---|---|---|---|---|---|---|
| **1.** | 0.957 | D-Sorbitol | $C_6H_{14}O_6$ | 182.0794 | 0.35 | Sugar alcohol |
| **2.** | 0.991 | Quinic acid | $C_7H_{12}O_6$ | 192.0633 | 0.25 | Polyphenol |
| **3.** | 4.702 | Epifisetinidol-4α-ol | $C_{15}H_{14}O_6$ | 290.0778 | 2.04 | Flavonoid (Polyphenol) |
| **4.** | 5.137, 6.152 | Epicatechin-(4β→6)-epicatechin-(2β→7,4β→8)-epicatechin | $C_{45}H_{36}O_{18}$ | 864.1879, 864.1914 | 0.60 | Proanthocyanidin |
| **5.** | 6.166, 6.761, 6.995, 7.559 | Proanthocyanidin A5' | $C_{30}H_{24}O_{12}$ | 576.1258, 576.1245, 576.1259, 576.1247 | 4.49 | Proanthocyanidin (polyphenol) |
| **6.** | 6.404, 6.533 | Butein 4'-arabinosyl-(1→4)-galactoside | $C_{26}H_{30}O_{14}$ | 566.1616, 566.1630 | 0.17 | Flavonoid glycoside |
| **7.** | 6.993 | 6-(3,4-Dihydroxyphenyl)-6a,12b-dihydro-3,10,11,12-tetrahydroxy-[2]benzopyrano[3,4-c]benzopyran-8(6H)-one | $C_{22}H_{16}O_9$ | 424.0783 | 0.14 | Flavonoid |
| **8.** | 6.711, 6.918, 7.470, 7.638, 7.993 | 1,3,4,5-Tetracaffeoylquinic acid | $C_{43}H_{36}O_{18}$ | 840.1905, 840.1909, 840.1925, 840.1893, 840.1889 | 1.00 | Chlorogenic acid derivative, polyphenol |
| **9.** | 7.363 | Lippioside I | $C_{25}H_{30}O_{13}$ | 538.1684 | 0.12 | Terpenoid glycoside |
| **10.** | 12.107 | C16 Sphinganine | $C_{16}H_{35}NO_2$ | 273.2665 | 7.50 | Sphingolipid / Glycoside |
| **11.** | 12.256 | Unknown compound 1 | - | 317.2913 | 1.58 | - |
| **12.** | 13.302 | Unknown compound 2 | - | 386.1691 | 2.24 | - |
| **13.** | 18.346 | Unknown compound 3 | - | 278.1503 | 3.02 | - |
| **14.** | 18.349 | Unknown compound 4 | - | 148.015 | 2.48 | - |
| **15.** | 20.066 | Unknown compound 5 | - | 657.5013 | 1.08 | - |
| **16.** | 20.136 | Unknown compound 6 | - | 596.4487 | 1.68 | - |
| **17.** | 20.207 | Unknown compound 7 | - | 569.4489 | 1.59 | - |
| **18.** | 20.266 | Unknown compound 8 | - | 508.3963 | 1.22 | - |
| **19.** | 21.139 | Momordicoside K | $C_{37}H_{60}O_9$ | 648.4217 | 0.07 | Triterpenoid saponin |

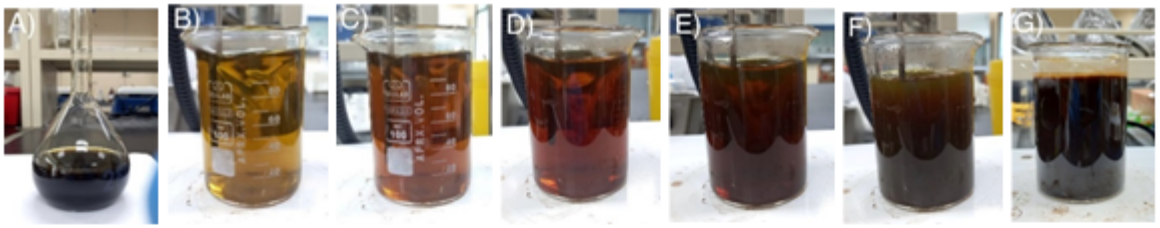


**Fig. 3:** (a) *A. densiflora* leaf extract. AD-AgNPs at (b) 10 min, (c) 20 min, (d) 30 min, (e) 1 h, (f) 2h, and (g) after pH adjustment.

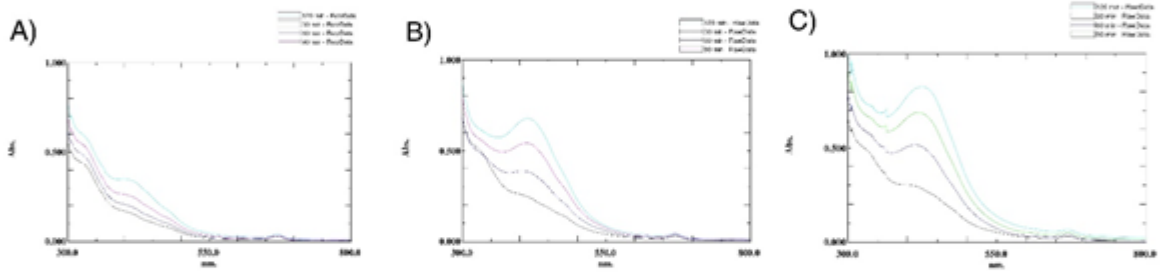


**Fig. 4:** Absorbance peaks of AD-AgNPs synthesised with (a) 1, (b) 5, and (c) 10 mM AgNO over time.

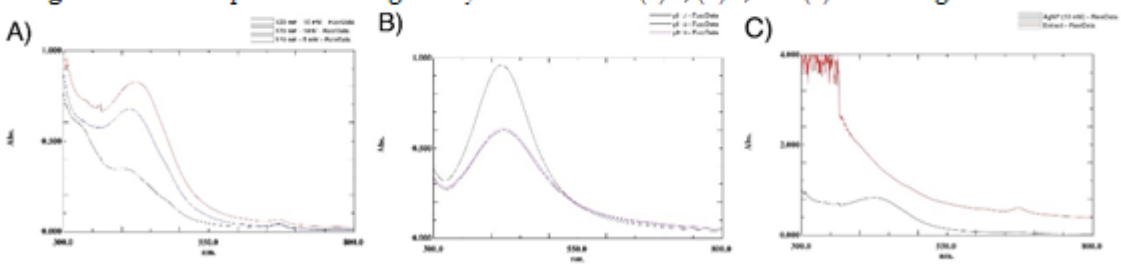


**Fig. 5: (a)** Absorbance peaks of AD-AgNPs synthesised with 1, 5, and 10 mM $AgNO_3$. (b) Absorbance peaks of AD-AgNPs synthesised at pH 7, 8, and 9. (c) Absorbance peaks of AD-AgNPs and plant extract.

UV–vis analysis

The formation of synthesised AD-AgNPs was further confirmed using UV–visible spectroscopy. Fig. 4 and 5 shows that peak absorbance increases as the reaction time increases. The characteristic peaks of AD-AgNPs synthesised with 1, 5, and 10 mM $AgNO_3$ after 2 hours synthesis (Fig. 4) were observed at wavelengths between 399–424 nm. This confirms the formation of AgNPs, as the SPR peak of AgNPs is typically falls within the 400–450 nm range (Sukweenadhi et al., 2021). The absorbance readings between the three samples of varying $AgNO_3$ concentration indicate that the sample synthesised with 10 mM $AgNO_3$ exhibits the highest absorbance peak, suggesting the highest yield compared to those synthesised with 1 and 5 mM $AgNO_3$. Consequently, 10 mM $AgNO_3$ was selected to investigate the effects of different pH levels on AgNP synthesis.

**Fig. 5 (b)** presents the absorbance peaks of AD-AgNPs synthesised at pH 7, 8, and 9. The sample synthesised at pH 7 showed the highest absorbance of 0.961 compared to pH 8 and 9 with absorbance of 0.593 and 0.604 respectively. Additionally, the absorbance peaks for pH 8 and 9 slightly decreased 30 minutes after pH adjustment, suggesting potential aggregation at higher pH levels. These findings were also observed in a previous study by Liaqat et al. (2022), where pH 7 was found to be the optimum pH for AgNP formation, and agglomeration was observed at very basic pH levels.

Furthermore, **Fig. 4** shows all samples exhibited two peaks: one within the 399–424 nm wavelength range, which is the characteristic peak of AgNP, and another minor peak between 611–671 nm, which may correspond to compounds in the *A. densiflora* extract. **Fig. 5 (c)** compares the UV peaks of the *A. densiflora* extract and AD-AgNPs, further confirming that the peak observed at ~600 nm originates from compounds in the extract.

*Particle size, and zeta potential analysis*

**Fig. 6** shows the size distribution of AD-AgNPs synthesised at varying $AgNO_3$ concentrations and pH levels, while **Fig. 7** presents their corresponding zeta potential measurements. As the $AgNO_3$ concentration increased, the particle size and polydispersity index (PDI) value decreased. According to H. B. Kim et al. (2024), a PDI value closer to 1 indicates polydisperse and aggregated particles, while a PDI between 0.1 and 0.4 suggests uniform size and low aggregation.

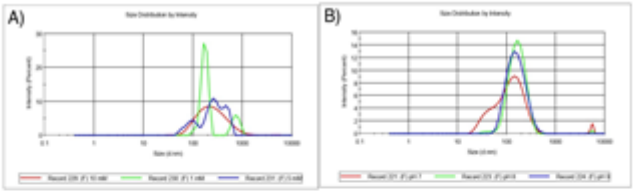


**Fig. 6:** Size distribution analysis of AD-AgNPs: (a) at different $AgNO_3$ concentrations and (b) at different pH levels.

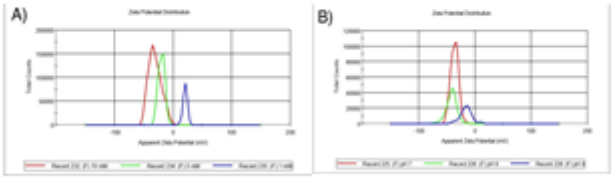


**Fig. 7:** Zeta potential analysis of AD-AgNPs: (a) at different $AgNO_3$ concentrations, and (b) at different pH levels.

Among all samples, AD-AgNPs synthesised at pH 9 exhibited the smallest particle size (139.8 nm) with a uniform distribution (PDI = 0.164), and the highest stability (-41.5 mV), as shown in **Table 2**. According to Liaqat et al. (2022), a minimum zeta potential of ±30 mV is required for a stable nanosuspension. The negative zeta potential suggests effective capping by phytocompounds present in the plant extract, leading to electrostatic repulsion between particles, which prevents agglomeration.

By comparing particles size and zeta potential measurements, it can be concluded that AD-AgNPs synthesised with 10 mM $AgNO_3$ at pH 9 exhibit the highest stability. However, at pH 7, the highest absorbance peak was observed in UV-Vis analysis, suggesting a high nanoparticle yield, despite the slightly larger particle size (153.1 nm), higher PDI (0.311), and lower zeta potential (-35.6 mV) compared to pH 9.

**Table 2:** Particle size and zeta potential of AgNPs.

| Variables | Z-Average (nm) | PDI | Zeta potential (mV) |
|---|---|---|---|
| 1 mM | 1652 | 1.000 | -17.1 |
| 5 mM | 629.5 | 0.591 | -19.9 |
| 10 mM | 198.1 | 0.271 | -31.0 |
| pH 7 | 153.1 | 0.311 | -35.6 |
| pH 8 | 177.2 | 0.308 | -18.3 |
| pH 9 | 139.8 | 0.164 | -41.5 |

*SEM and EDX analysis*

Among the tested samples, AD-AgNPs synthesised at pH 7 were selected for further analysis, as they exhibited the highest absorbance in UV spectroscopy analysis, while maintaining a fair

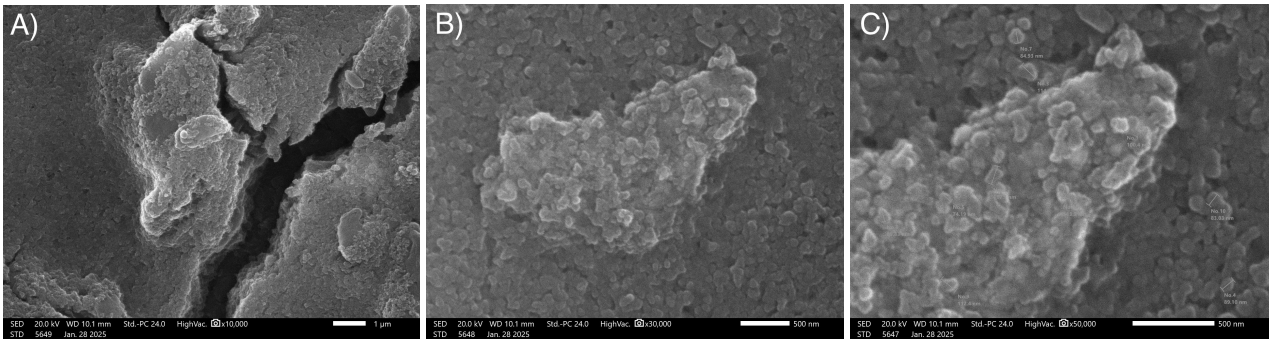


**Fig. 8:** SEM profile of AD-AgNPs at (a) 10 000, (b) 30 000, and (c) 50 000 magnifications.

particle size and good stability.

SEM profiles of AD-AgNPs under different magnifications are depicted in **Fig. 8.** The images show that AgNPs have a spherical-like shape with an average size of 96.06 nm but appear highly aggregated. Although the synthesised AgNPs are considerably small and within the nano range, the significant aggregation has led to the formation of larger structures. These findings suggest that while *A. densiflora* leaf extract demonstrates strong reducing capabilities for AgNP synthesis, its stabilising properties appear to be insufficient, leading to nanoparticle aggregation.

EDX analysis identified the purity, and the complete chemical composition of elements present in AD-AgNPs, as shown in **Fig. 9**. The analysis revealed the significant proportions of silver (68.25%) alongside oxygen (31.75%). The presence of oxygen is likely due to the oxidation of AgNPs or the strong binding of organic compounds from *A. densiflora* extract, capping the nanoparticle surface (Femi-Adepoju et al., 2019).

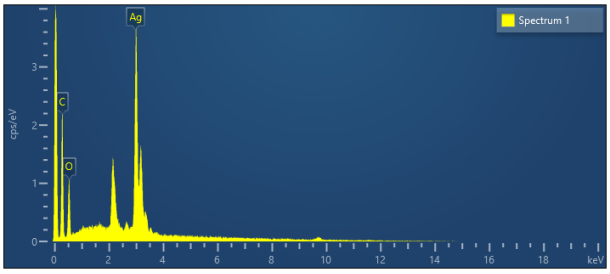


**Fig. 9:** EDX profile of AD-AgNPs with percentage weight of each element.

*XRD analysis*

The XRD spectrum (**Fig. 10**) revealed distinct peaks at 2θ angles of 38.14°, 44.07°, 64.49°, 77.31°, and 81.56°, corresponding to the (111), (200), (220), (311), and (222) lattice planes of the face-centred cubic (FCC) structure of AgNPs. These findings align with previously reported values for crystalline AgNPs (Lanje et al., 2010; Revathi et al., 2024) confirming the crystalline nature of AD-AgNPs. The crystallite sizes were calculated, and the results are summarised in **Table 3**, with an average size of 6.94 nm.

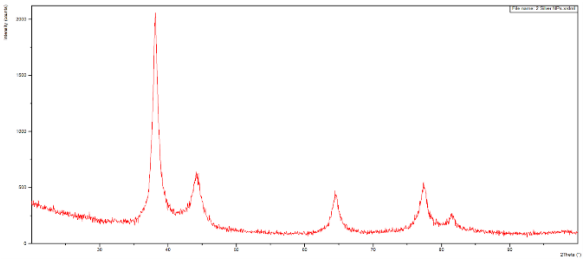

**Fig. 10:** The XRD spectrum revealed distinct peaks at 2θ angles of 38.14°, 44.07°, 64.49°, 77.31°, and 81.56°, corresponding to the (111), (200), (220), (311), and (222) lattice planes of the face-centred cubic (FCC) structure of AgNPs.

**Table 3:** The crystallite size of AD-AgNPs.

| 2θ [°] | hkl | FWHM Left [°2θ] | d-spacing [Å] | D (nm) |
|---|---|---|---|---|
| 38.1356° | 111 | 0.9079 | 2.35791 | 9.67 |
| 44.0680° | 200 | 1.7884 | 2.05327 | 5.00 |
| 64.4886° | 220 | 1.2590 | 1.44378 | 7.79 |
| 77.3120° | 311 | 1.6769 | 1.23318 | 6.34 |
| 81.5649° | 222 | 1.8629 | 1.17929 | 5.88 |
| | | $D_{average}$ (nm) | | 6.94 |

*TGA*

The TGA profile **(Fig. 11)** shows that AD-AgNPs exhibited a slight weight loss from room temperature to 100°C, which may be attributed to the evaporation of surface moisture. The sample then gradually degraded, and by 290°C, 50% of the it had already decomposed. A significant weight loss was observed starting at 300°C, with complete decomposition occurring at 371°C. Previous studies have associated weight loss between 100–350°C with the degradation of organic biomolecules, such as phenolics and flavonoids, which serve as capping agents on AgNPs (David & Moldovan, 2020). The melting point of pure silver is reported to be 960.54°C (Sampaio & Viana, 2018). However, the

complete degradation of AD-AgNPs observed at 371°C suggests a few possible explanations.

Firstly, AD-AgNPs may contain only a minimal amount of pure silver, with an excessive presence of organic capping molecules. Moreover, this analysis was performed using a limited sample size, which may have influenced the results. Given the already small initial weight and the minimal amount of pure silver, any residual mass may have been below the detection limit of the instrument. Therefore, for more accurate quantification, future TGA experiments should be conducted with a larger sample size.

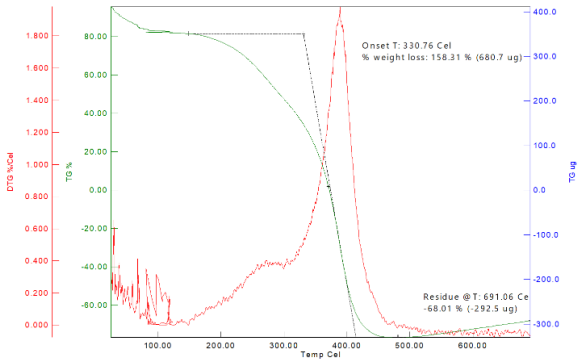


**Fig. 11:** TGA graph of AD-AgNPs. The initial sample weight was 0.43 mg, heated from room temperature to 700 °C at a heating rate of 10 °C/min.

*FTIR analysis*

FTIR analysis was carried out to identify the functional groups responsible for AgNP formation by examining shifts in spectral bands between the plant extracts and the synthesised AgNPs (Dhaka et al., 2023). **Fig. 12** presents a comparison of the IR spectra of *A. densiflora* leaf extract and synthesised AgNPs.

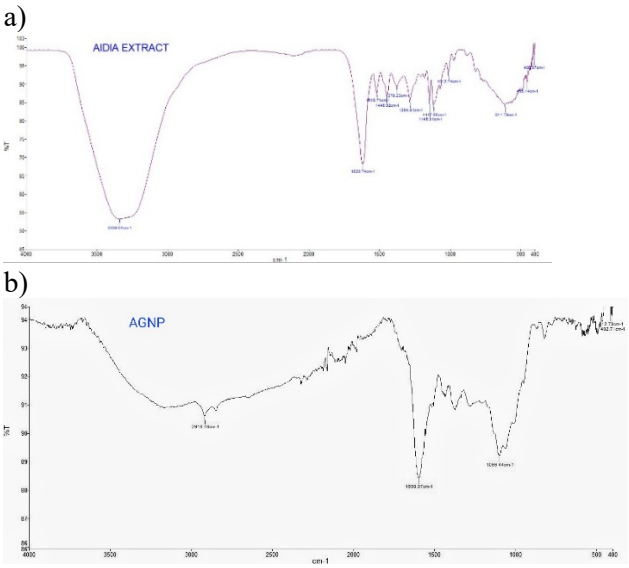


**Fig. 12:** FTIR profile of (a) *A. densiflora* leaf extract, and (b) AD-AgNPs. Spectra were recorded using an FTIR spectrometer in the range of 4000–400 $cm^{-1}$ in Attenuated Total Reflectance (ATR) mode.

The FTIR spectrum of the extract revealed an O–H stretching vibration at 3339 $cm^{-1}$, which disappeared after AgNP synthesis. Instead, a new peak emerged at 2918 $cm^{-1}$, suggesting strong interactions between hydroxyl groups and AgNPs. Additionally, a peak shift from 1620 $cm^{-1}$ to 1598 $cm^{-1}$ indicates C=O stretching from the carbonyl group, while another shift from 1117 $cm^{-1}$ to 1099

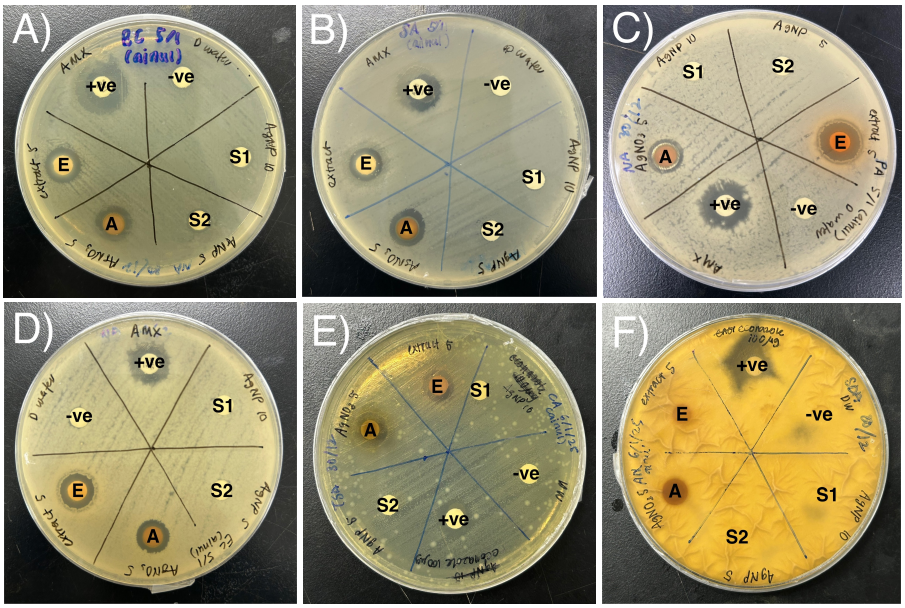


**Fig. 13:** Antibacterial activity of AD-AgNPs, *A. densiflora* leaf extract, and $AgNO_3$ against (a) *B. subtilis*, (b) *S. aureus*, (c) *E. coli*, (d) *P. aeruginosa*, (e) *C. albicans*, and (f) *A. niger*. (S1: 10 mg/mL AD-AgNPs, S2: 10 mg/mL AD-AgNPs, E: *A. densiflora* extract (5 mg/mL), A: $AgNO_3$ (5 mg/mL), -ve: Negative control (distilled water), and +ve: Positive control).

$cm^{-1}$ suggests C–O stretching from ether or alcohol groups. These spectral changes indicate interactions between phytochemicals and AgNPs. The observed shifts suggest that phytocompounds from *A. densiflora,* particularly those containing alcohol, alkene, carbonyl, and ether functional groups, may play a role in the reduction and stabilisation of AgNPs. These findings align with previous studies that have also identified similar functional groups in plant-mediated AgNPs (Cherukuri & Kammela, 2022; Khan et al., 2023). Furthermore, the presence of characteristic peaks at 2918.43 $cm^{-1}$, 1598.97 $cm^{-1}$, and 1099.44 $cm^{-1}$ in the IR spectrum of AD-AgNPs supports the assumption that biomolecules from the plant extract are bonded to the surface of AgNPs, acting as capping agents and influencing nanoparticle stability (Asong et al., 2023).

*Antimicrobial assay*

**Fig. 13** shows ZOI for all microbes; however, excessive fungal overgrowth in *A. niger* (**Fig. 13(f)**) prevented accurate measurements despite multiple experimental repetitions. This suggests the disc diffusion method may be unsuitable for this strain due to its rapid mycelial growth.

**Fig. 14** shows that AD-AgNPs did not exhibit significant inhibition against the tested microbes. Interestingly, $AgNO_3$ solution and the plant extract exhibited good antimicrobial activity, suggesting that although both precursors possessed antimicrobial properties, the synthesised AgNPs did not retain or enhance these effects. This contradicts the findings of Roy et al. (2019), who reported that when capping agents exhibit antimicrobial properties, a synergistic effect between the nanoparticles and the phytocompounds may occur.

Several factors may contribute to these findings, primarily the aggregation and stability of the synthesised AgNPs. According to Bruna et al. (2021), AgNPs size and surface characteristics significantly influence the release rate of silver ions, thereby affecting antimicrobial properties. A study by Korshed et al. (2019) demonstrated that smaller AgNPs exhibit stronger antimicrobial effects due to their larger surface area, which facilitates direct interaction with bacterial cells. Additionally, surface charge plays a crucial role in nanoparticle stability. AgNPs with low stability tend to aggregate, forming larger particles, which in turn reduces their antimicrobial efficacy (Bruna et al., 2021). In this study, SEM images revealed significant aggregation of AD-AgNPs. Furthermore, after the centrifugation step during synthesis, the resulting pellet appeared highly aggregated, requiring an additional 24-hour stirring to improve dispersion. This further proves the tendency of AD-AgNPs to aggregate, potentially leading to larger particle sizes and reduced antimicrobial effectiveness.

The antimicrobial effect of silver nanoparticles primarily results from the continuous release of silver ions ($Ag^+$). Due to electrostatic attractions, $Ag^+$ interacts with negatively charged molecules on bacterial cell walls, leading to membrane disruption, and eventually cell death (Yin et al., 2020). A previous study by Kim et al. (2022) observed low antimicrobial activity in pine needle extract-mediated AgNPs, presuming this to be excessive surface capping of polyphenols which may have reduced the electrostatic interaction between the nanoparticles and bacterial cells. Similarly, in this study, EDX analysis detected a high oxygen content in the AD-AgNPs, suggesting extensive phytochemical capping. This excessive surface capping may have prevented the release of $Ag^+$, thereby limiting the antimicrobial activity of AD-AgNPs.

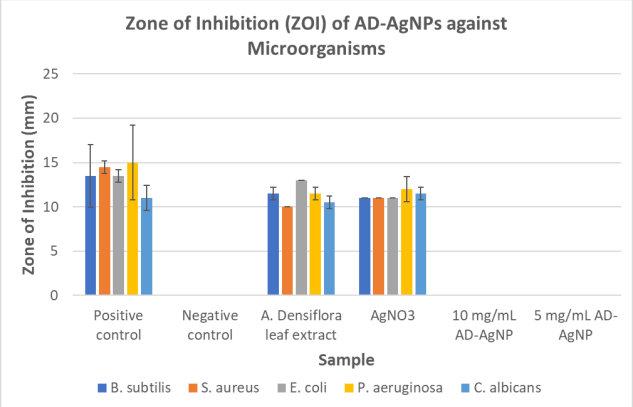


**Fig. 14:** Zone of Inhibitions of AD-AgNPs against different microorganisms.

*Cytotoxicity assay*

The MCF-7 cells were exposed to various concentrations of AD-AgNPs for 24 hours, and cytotoxicity was assessed using the MTT assay. **Fig. 15** illustrates the cytotoxic effects of AD-AgNPs, $AgNO_3$, and tamoxifen (positive control) at various concentrations. AD-AgNPs exhibited a low cytotoxic activity as even at the highest concentration (5 mg/mL), the cell viability remained relatively high (81%). Statistical analysis ($p > 0.05$) indicates no significant difference among treatments, suggesting that all treatments including

the positive control, exhibited low cytotoxic effects against MCF-7 cells.

While a dose-dependent trend was expected, fluctuations were observed across concentrations. The unexpected decrease in cell viability at lower concentrations of AD-AgNPs (79% at 0.625 mg/mL, 75% at 0.312 mg/mL) suggests inconsistencies, possibly due to uneven nanoparticle dispersion, slight variations in cell counts, or potential contamination during handling.

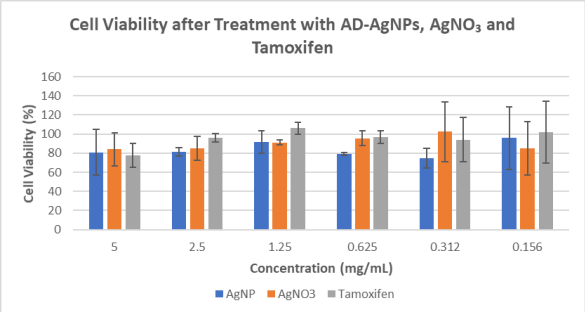


**Fig. 15:** Percentage cell viability of MCF-7 cell after treated with AD-AgNPs, $AgNO_3$, and *A. densiflora* leaf extract using MTT assay.

Previous studies have demonstrated that plant extract-mediated AgNPs exhibit strong anticancer properties against various human cancer cell lines, including MCF-7 (human breast adenocarcinoma) (Yeşilot & Dönmez, 2021), HeLa (human cervical cancer, ATCC CCL-2), A375, and SK-MEL-3 (human melanoma) (Radzikowska-Büchner et al., 2023). Therefore, low cytotoxicity of AD-AgNPs against MCF-7 cells may be attributed to aggregation, surface capping effects, or low bioavailability, which require further investigation.

## Conclusion

This study demonstrates that AgNPs can be successfully synthesised using *A. densiflora* leaf extract, as confirmed by UV-vis spectroscopy, EDX, and XRD. LC-MS/QTOF identified several possible compounds that may play a role in the synthesis, including flavonoids, proanthocyanidins, terpenoids, steroids, and sugar alcohols. FTIR revealed the presence of alcohol, alkene, carbonyl, and ether functional groups on AD-AgNPs, which are most likely compounds from the extract acting as reducing and capping agents.

The average particle size was found to be relatively small (96.06 nm) with a good zeta potential value (-35.6 mV). XRD confirmed their crystalline structure, while SEM images revealed significant aggregation. The antimicrobial assay showed no ZOI for AD-AgNPs, whereas $AgNO_3$ and the plant extract exhibited some activity, suggesting that the synthesised AgNPs failed to retain or enhance the antimicrobial properties of their precursors.

The findings of this study suggest that, although AgNPs were successfully synthesised, their high level of aggregation may have reduced their biological activity. Future studies should focus on optimising the synthesis process to improve AgNP stability, minimise aggregation, and enhance biological activity.

## Authors contributions

**A.H.:** Investigations, methodology, writing—original draft. **M. T., M.T.M.J.:** Supervision, funding acquisition. **J.M.J.:** Funding acquisition. **D.D., J.K.:** reviewing the draft. All authors have read and agreed to the published version of the manuscript.

## Acknowledgements

We would like to thank the Kulliyyah of Pharmacy, the International Islamic University Malaysia for facility and support.

## Conflict of interest

The authors declare no conflict of interest.

## Declaration of generative AI and AI-assisted technologies in the writing process

During the preparation of this work the author used ChatGPT in order to improve readability and language. After using this tool/service, the author reviewed and edited the content as needed and take full responsibility for the content of the publication.

## References

Akhter, M. S., Rahman, M. A., Ripon, R. K., Mubarak, M., Akter, M., Mahbub, S., Al Mamun, F., & Sikder, M. T. (2024). A systematic review on green synthesis of silver nanoparticles using plants extract and their bio-medical applications. *Heliyon*, *10*(11), e29766. https://doi.org/10.1016/j.heliyon.2024.e29766

Alharbi, N. S., Alsubhi, N. S., & Felimban, A. I. (2022). Green synthesis of silver nanoparticles using medicinal plants: Characterization and

application. *Journal of Radiation Research and Applied Sciences*, *15*(3), 109–124. https://doi.org/10.1016/j.jrras.2022.06.012

Anokwah, D., Asante-Kwatia, E., Mensah, A. Y., Danquah, C. A., Harley, B. K., Amponsah, I. K., & Oberer, L. (2021). Bioactive constituents with antibacterial, resistance modulation, anti-biofilm formation and efflux pump inhibition properties from Aidia genipiflora stem bark. *Clinical Phytoscience*, *7*(1). https://doi.org/10.1186/s40816-021-00266-4

Arsène, M. M. J., Viktorovna, P. I., Alla, M., Mariya, M., Nikolaevitch, S. A., Davares, A. K. L., Yurievna, M. E., Rehailia, M., Gabin, A. A., Alekseevna, K. A., Vyacheslavovna, Y. N., Vladimirovna, Z. A., Svetlana, O., & Milana, D. (2023). Antifungal activity of silver nanoparticles prepared using Aloe vera extract against Candida albicans. *Veterinary World*, *16*(1), 18–26. https://doi.org/10.14202/vetworld.2023.18-26

Asif, M., Yasmin, R., Asif, R., Ambreen, A., Mustafa, M., & Umbreen, S. (2022). Green Synthesis of Silver Nanoparticles (AgNPs), Structural Characterization, and their Antibacterial Potential. *Dose-Response*, *20*(1), 1–11. https://doi.org/10.1177/15593258221088709

Asong, J. A., Frimpong, E. K., Seepe, H. A., Katata-Seru, L., Amoo, S. O., & Aremu, A. O. (2023). Green Synthesis of Characterized Silver Nanoparticle Using Cullen tomentosum and Assessment of Its Antibacterial Activity. *Antibiotics (Basel, Switzerland)*, *12*(2). https://doi.org/10.3390/antibiotics12020203

Awang-Jamil, Z., Basri, A. M., Ahmad, N., & Taha, H. (2019). Phytochemical analysis, antimicrobial and antioxidant activities of Aidia borneensis leaf extracts. *Journal of Applied Biology and Biotechnology*, *7*(5), 92–97. https://doi.org/10.7324/JABB.2019.70515

Bruna, T., Maldonado-bravo, F., Jara, P., & Caro, N. (2021). Silver Nanoparticles and Their Antibacterial Applications. *International Journal of Molecular Sciences*, *22*(7202). https://doi.org/https://doi.org/10.3390/ijms22137202

Cherukuri, A., & Kammela, P. R. (2022). Green Synthesis of Silver Nanoparticles, Characterization and Antimicrobial Activity Studies by Using Gomphrena Serrata Leaf Extract. *Journal of Scientific Research*, *66*(01), 358–362. https://doi.org/10.37398/jsr.2022.660138

David, L., & Moldovan, B. (2020). Green synthesis of biogenic silver nanoparticles for efficient catalytic removal of harmful organic dyes. *Nanomaterials*, *10*(2). https://doi.org/10.3390/nano10020202

Eze, F. N., Tola, A. J., Nwabor, O. F., & Jayeoye, T. J. (2019). Centella asiatica phenolic extract-mediated bio-fabrication of silver nanoparticles: Characterization, reduction of industrially relevant dyes in water and antimicrobial activities against foodborne pathogens. *RSC Advances*, *9*(65), 37957–37970. https://doi.org/10.1039/c9ra08618h

Fadhillah, I. R., Taher, M., Nur, M., & Susanti, D. (2024). *Green-synthesized silver nanoparticles from Anisophyllea corneri leaf extract and its antimicrobial and cytotoxic activities*. *4*, 103–115. https://doi.org/10.31436/jop.v4i1.265

Femi-Adepoju, A. G., Dada, A. O., Otun, K. O., Adepoju, A. O., & Fatoba, O. P. (2019). Green synthesis of silver nanoparticles using terrestrial fern (Gleichenia Pectinata (Willd.) C. Presl.): characterization and antimicrobial studies. *Heliyon*, *5*(4), e01543. https://doi.org/10.1016/j.heliyon.2019.e01543

Jalab, J., Abdelwahed, W., Kitaz, A., & Al-Kayali, R. (2021). Green synthesis of silver nanoparticles using aqueous extract of Acacia cyanophylla and its antibacterial activity. *Heliyon*, *7*(9), e08033. https://doi.org/10.1016/j.heliyon.2021.e08033

Karu, E., Magaji, B., Shehu, Z., & Abdulsalam, H. (2020). Green Synthesis of Silver Nanoparticles From Solenostemon Monostachyus Leaf Extract and In Vitro Antibacterial and Antifungal Evaluation. *European Journal of Advanced Chemistry Research*, *1*(4), 1–5. https://doi.org/10.24018/ejchem.2020.1.4.11

Khan, J., Naseem, I., Bibi, S., Ahmad, S., Altaf, F., Hafeez, M., Almoneef, M. M., & Ahmad, K. (2023). Green Synthesis of Silver Nanoparticles (Ag-NPs) Using Debregeasia Salicifolia for Biological Applications. *Materials*, *16*(1).

https://doi.org/10.3390/ma16010129

Kim, H. B., You, H. S., Ryu, S. ji, Lee, H. Y., & Baek, J. S. (2024). Green synthesis of silver nanoparticles from mulberry leaf through hot melt extrusion: Enhanced antioxidant, antibacterial, anti-inflammatory, antidiabetic, and anticancer properties. *Food Hydrocolloids for Health*, *6*(May), 100184. https://doi.org/10.1016/j.fhfh.2024.100184

Kim, Y. H., Bang, Y. J., Yoon, K. S., Priyadarshi, R., & Rhim, J. W. (2022). Pine Needle (Pinus densiflora) Extract-Mediated Synthesis of Silver Nanoparticles and the Preparation of Carrageenan-Based Antimicrobial Packaging Films. *Journal of Nanomaterials*, *2022*. https://doi.org/10.1155/2022/8395302

Korshed, P., Li, L., Liu, Z., Mironov, A., & Wang, T. (2019). Size-dependent antibacterial activity for laser-generated silver nanoparticles. *Journal of Interdisciplinary Nanomedicine*, *4*(1), 24–33. https://doi.org/10.1002/jin2.54

Lanje, A. S., Sharma, S. J., & Pode, R. B. (2010). Synthesis of silver nanoparticles: a safer alternative to conventional antimicrobial and antibacterial agents. *Journal of Chemical and Pharmaceutical Research*, *2*(3), 675–684.

Liaqat, N., Jahan, N., Khalil-ur-Rahman, Anwar, T., & Qureshi, H. (2022). Green synthesized silver nanoparticles: Optimization, characterization, antimicrobial activity, and cytotoxicity study by hemolysis assay. *Frontiers in Chemistry*, *10*(August), 1–13. https://doi.org/10.3389/fchem.2022.952006

Nguyen, N. P. U., Dang, N. T., Doan, L., & Nguyen, T. T. H. (2023). Synthesis of Silver Nanoparticles: From Conventional to 'Modern' Methods—A Review. *Processes*, *11*(9). https://doi.org/10.3390/pr11092617

Pallavi, S. S., Rudayni, H. A., Bepari, A., Niazi, S. K., & Nayaka, S. (2022). Green synthesis of Silver nanoparticles using Streptomyces hirsutus strain SNPGA-8 and their characterization, antimicrobial activity, and anticancer activity against human lung carcinoma cell line A549. *Saudi Journal of Biological Sciences*, *29*(1), 228–238. https://doi.org/10.1016/j.sjbs.2021.08.084

Radzikowska-Büchner, E., Flieger, W., Pasieczna-Patkowska, S., Franus, W., Panek, R., Korona-Głowniak, I., Suśniak, K., Rajtar, B., Świątek, Ł., Żuk, N., Bogucka-Kocka, A., Makuch-Kocka, A., Maciejewski, R., & Flieger, J. (2023). Antimicrobial and Apoptotic Efficacy of Plant-Mediated Silver Nanoparticles. *Molecules*, *28*(14). https://doi.org/10.3390/molecules28145519

Revathi, S., Sutikno, S., Hasan, A. F., Altemimi, A. B., Hamed, Q., Phillips, A. J., & Ali, M. (2024). Green synthesis and characterization of silver nanoparticles ( AgNP ) using Acacia nilotica plant extract and their anti-bacterial activity. *Food Chemistry Advances*, *4*(December 2023), 100680. https://doi.org/10.1016/j.focha.2024.100680

Roy, A., Bulut, O., Some, S., Mandal, A. K., & Yilmaz, M. D. (2019). Green synthesis of silver nanoparticles: Biomolecule-nanoparticle organizations targeting antimicrobial activity. *RSC Advances*, *9*(5), 2673–2702. https://doi.org/10.1039/c8ra08982e

Safarpoor, M., Ghaedi, M., Asfaram, A., Yousefi-Nejad, M., Javadian, H., Zare Khafri, H., & Bagherinasab, M. (2018). Ultrasound-assisted extraction of antimicrobial compounds from Thymus daenensis and Silybum marianum: Antimicrobial activity with and without the presence of natural silver nanoparticles. *Ultrasonics Sonochemistry*, *42*(October 2017), 76–83. https://doi.org/10.1016/j.ultsonch.2017.11.001

Sampaio, S., & Viana, J. C. (2018). Production of silver nanoparticles by green synthesis using artichoke (Cynara scolymus L.) aqueous extract and measurement of their electrical conductivity. *Advances in Natural Sciences: Nanoscience and Nanotechnology*, *9*(4). https://doi.org/10.1088/2043-6254/aae987

Singh, J., Dutta, T., Kim, K. H., Rawat, M., Samddar, P., & Kumar, P. (2018). "Green" synthesis of metals and their oxide nanoparticles: Applications for environmental remediation. *Journal of Nanobiotechnology*, *16*(1), 1–24. https://doi.org/10.1186/s12951-018-0408-4

Sukweenadhi, J., Setiawan, K. I., Avanti, C., Kartini, K., Rupa, E. J., & Yang, D. C. (2021). Scale-up of green synthesis and characterization of

silver nanoparticles using ethanol extract of Plantago major L. leaf and its antibacterial potential. *South African Journal of Chemical Engineering*, *38*(April), 1–8. https://doi.org/10.1016/j.sajce.2021.06.008

Sundar, M., Rajagopal, G., Nivetha, A., Prabu Kumar, S., & Muthukumar, S. (2024). Phyto-Mediated Green Synthesis of Silver Nanoparticles Using an Aqueous Leaf Extract of Momordica cymbalaria: Antioxidant, Cytotoxic, Antibacterial, and Photocatalytic Properties. *Separations*, *11*(2). https://doi.org/10.3390/separations11020061

Vanlalveni, C., Lallianrawna, S., Biswas, A., Selvaraj, M., Changmai, B., & Rokhum, S. L. (2021). Green synthesis of silver nanoparticles using plant extracts and their antimicrobial activities: a review of recent literature. *RSC Advances*, *11*(5), 2804–2837. https://doi.org/10.1039/d0ra09941d

Velidandi, A., Dahariya, S., Pabbathi, N. P. P., Kalivarathan, D., & Baadhe, R. R. (2020). A review on synthesis, applications, toxicity, risk assessment and limitations of plant extracts synthesized silver nanoparticles. *NanoWorld Journal*, *6*(3), 35–60. https://doi.org/10.17756/nwj.2020-079

Yeşilot, Ş., & Dönmez, S. (2021). Cytotoxic effect of green synthesized silver nanoparticles with Salvia officinalis on MCF-7 human breast cancer. *Turkish Journal of Health Science and Life*, *4*, 133–139.

Yin, I. X., Zhang, J., Zhao, I. S., Mei, M. L., Li, Q., & Chu, C. H. (2020). The antibacterial mechanism of silver nanoparticles and its application in dentistry. *International Journal of Nanomedicine*, *15*, 2555–2562. https://doi.org/10.2147/IJN.S246764

Zuhrotun, A., Oktaviani, D. J., & Hasanah, A. N. (2023). Biosynthesis of Gold and Silver Nanoparticles Using Phytochemical Compounds. *Molecules*, *28*(7). https://doi.org/10.3390/molecules28073240